Sensitivity Analysis for Capillary Pressure Data from Centrifuge Considering Different Rotation Speed Range, Centrifuges Models and Sample Size

Alessandra S. Winter [1,2,*], *Andre* L. M.Compan [3], *Flavia* B. De Andrade [3], and *Rosangela* B. Z. L. Moreno [1,2]

[1] School of Mechanical Engineering (FEM), Universidade Estadual de Campinas (UNICAMP)
[2] Centro de Estudos de Energia e Petróleo (CEPETRO), Universidade Estadual de Campinas (UNICAMP)
[3] Centro de Pesquisas, Desenvolvimento e Inovação Leopoldo Américo Miguez de Mello (CENPES/PDIEP/TAE/TRESP), Petrobras

Abstract. Capillary pressure is a fundamental reservoir property that must be understood to ensure efficient oil exploration. It refers to the pressure difference at the interface between two immiscible fluids present in the pore spaces of a porous medium, typically oil and water in the context of hydrocarbon reservoirs. This pressure difference arises due to capillary forces acting at the fluid-fluid and fluid-rock interfaces. Depending on the pore configuration and rock wettability, capillary pressure can significantly affect fluid displacement conditions, resulting in high residual or remaining oil saturation. Centrifuge capillary pressure experiments are valuable tools for understanding fluid behavior in porous rock formations. These tests expose rock samples to high centrifugal forces to simulate subsurface conditions and analyze capillary pressure phenomena. The data obtained provide crucial insights into fluid behavior, saturation distribution, and the relative permeability of reservoir rocks. A good approach to ensure reliability of results is to conduct analyses in duplicate. This helps assess the reproducibility of the data and account for potential variations in sample properties, providing a more robust interpretation of the results. However, conducting tests on reservoir rocks in duplicate often raises concerns about result reproducibility, as it is impossible to ensure that samples share identical initial conditions. Mineralogical heterogeneity and variations in pore structure can significantly impact experimental outcomes. In this context, error bars enhance result interpretation by accounting for natural sample variability, thereby improving the reliability of analyses, particularly in reservoir modeling and simulation. Centrifuge equipment can vary the rotation speed range, core bottom, volume resolution, and maximum sample size. This study presents a sensitivity analysis of capillary pressure data obtained from centrifuge tests, considering four centrifuge models. The resolution of measured variables was used to evaluate the propagated uncertainty on obtained results. The investigation examines how different rotation speeds and sample sizes influence the accuracy and reliability of capillary pressure measurements across various equipment, according to the specifications described in the manuals. By systematically analyzing these factors, this study provides valuable insights into the robustness and sensitivity of capillary pressure data under varying experimental conditions. Ultimately, a comparison is presented between the relative uncertainties of capillary pressure curves obtained using different high-speed centrifuges. These findings contribute to the refinement and optimization of centrifuge testing methodologies, leading to more accurate reservoir characterization and improved oil recovery strategies.

1 Introduction

Capillary pressure plays a critical role in reservoir performance by influencing key factors such as initial fluid saturation, fluid distribution, and overall recovery efficiency. Expressed as the pressure difference across the interface between two immiscible fluids, capillary pressure effects are particularly significant during enhanced oil recovery processes [1]. In the context of petroleum reservoir exploration, a thorough understanding of capillary pressure distribution is fundamental for estimating initial fluid saturations and consequently, the original hydrocarbon volumes in place. The experimental test consists in measuring the pressure applied to the rock-fluid system and the corresponding displaced fluid volume, allowing to plot the capillary pressure versus the rock fluid saturation. The capillary pressure curves are significantly influenced by rock heterogeneity and wettability. It depends on pore size distribution, interfacial tension, interactions between rock and fluids, and saturation history [2]. When the wetting phase, typically water or brine, is displaced by the non-wetting phase, typically dead oil, mineral oil, or gas (e.g., air), the process is called drainage. In this case, as capillary pressure increases, the saturation of the wetting phase decreases. During drainage, beyond a certain

* Corresponding author: awinter@unicamp.br

capillary pressure, the non-wetting phase cannot displace the wetting phase anymore, and the saturation at which that occurs is known as the irreducible saturation of the wetting phase. In the imbibition process, the opposite occurs, where the saturation of the phase that wets the rock surface increases as capillary pressure increases. In heterogeneous systems, such as Brazilian pre-salt rocks with large variations in pore diameter, substantial amounts of oil can be left behind during fluid displacement due to the magnitude of capillary effects. Then, the understanding of the relationship between capillary pressure and saturation and their accurate experimental measurement are essential in immiscible displacement theory [3].

There are several methods to obtain petroleum capillary pressure curves, in both drainage and imbibition cycles, from laboratory experiments. The Porous Plate Method, Mercury Injection Capillary Pressure (MICP), and Centrifuge Method are commonly used techniques [4]. Each method has its advantages and limitations, and the choice depends on factors such as the rock lithology, fluid properties, and experimental conditions.

The Porous Plate Method entails placing one end of the rock sample in capillary contact with a saturated porous plate or semi-permeable membrane and applying step-wise increasing gas or oil pressure to the open surface(s) not in contact with the plate. At each applied pressure, the oil or gas will fill all pore throats (as well as the larger pore spaces controlled by those throats) with a radius equivalent to or larger than the applied pressure [5]. The capillary pressure curves can then be obtained by measuring the pressure at each stage as a function of the saturation. Equilibration times during porous plate tests can be substantial, often requiring extended periods to achieve equilibrium.

The Mercury Injection Capillary Pressure (MICP) involves mercury (Hg) injection into a rock sample under increasing pressure; while measuring the volume of the mercury that fills the pore space. MICP is a fast technique and also provides detailed information about pore-throat size distribution and pore connectivity. A wide range of pore sizes can be characterized with high resolution and the method can be applied to various rock types. Although MICP is fast technique to quantify the pore space it cannot determine accurate irreducible wetting saturation [6], and requires strict health, safety and environmental standards [7, 8]. To convert data from the Hg/air system to the water/oil system it is necessary to account for interfacial properties and contact angles of the respective systems through capillary pressure normalization. Consequently, it is therefore challenging to utilize the results obtained from this method to accurately predict the behavior in an oil-water system [3].

Despite limitations in test temperature, pore pressure, and the use of live fluids under reservoir conditions, the Centrifuge Method generates high capillary pressures through centrifugal force and remains a reliable technique for determining capillary pressure in rocks. This method has been used to measure capillary pressure in water-wet and oil-wet carbonate core plugs, aiming to achieve hydrostatic saturation equilibrium according wettability preference and absolute permeability [9]. In practice, rock samples are placed in a centrifuge cell, and the centrifugal force is applied to the sample so part of the fluid filling the rock pores is replaced by the displacing fluid. Different fluids are injected into the sample and the resulting capillary pressures are measured. The centrifugal force acting on the sample varies along its length, leading to corresponding variations in both capillary pressure and fluid saturation throughout the sample. Thus, the average saturation of the sample needs to be determined at each speed increment.

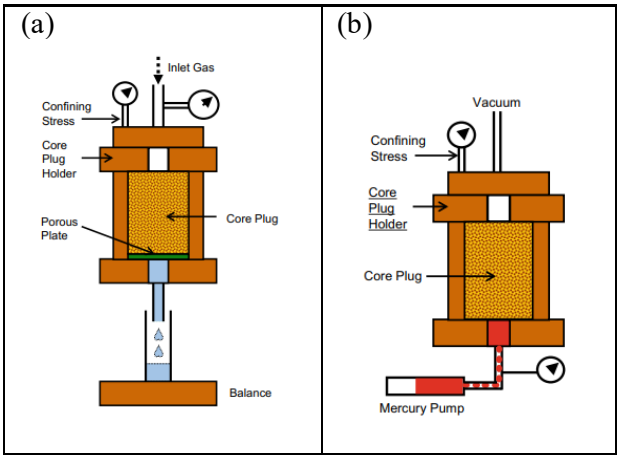

Fig. 1. Capillary pressure determination experiment: (a) Porous plate experiment and (b) Mercury injection experiment [10].

The experimental method selection depends on factors such as rock lithology and properties, fluid properties and experimental conditions. According to Christiansen [11], high-quality data resulting from centrifuge experiments are dependent on accurate measurements of spin rates and produced volumes, rock porosity and dimensions, and fluid densities, as well as good temperature control. Thus, sensitivity analysis of data obtained and used as input parameters in tests is crucial to ensure that the resulting capillary pressure curves accurately reflect the real behavior of the studied system.

The centrifuge method offers advantages such as shorter testing time compared to the porous plate method, good accuracy, and a non-destructive approach, as well as the possibility of using reservoir fluids such as brine and oil under room pressure conditions. The high speed centrifuges can reach high capillary pressures, allowing for fluid replacement even in the small pores of the rock sample, reaching low residual saturations. However, when dealing with highly friable samples or those containing fractures, it is important to exercise caution when employing the centrifuge method, as increased rotation speed can pose a risk of rock fracturing.

By analyzing the capillary pressure data, petroleum engineers can better understand how fluids flow through the porous media under various conditions, including different rock types, wettability and fluid compositions. Nevertheless, to render the data acquired from centrifuge experiments applicable in simulating and comprehending

reservoirs behavior, theoretical expressions must be fitted to experimental data using approximation or regression techniques to establish a correlation between local capillary pressure and local saturation. Determining the optimal approach for this process remains a challenge, despite its longstanding use in the oil industry. Several studies have tackled the challenge of converting centrifuge results into capillary pressure curves, proposing various methodologies for this transformation [12-19].

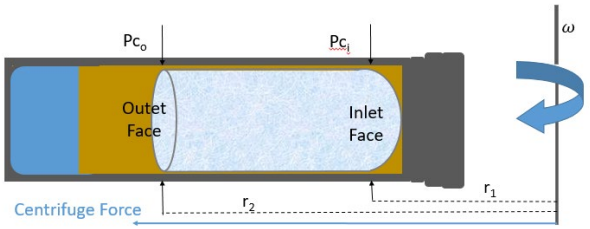

Fig. 2. Diagram of Drainage centrifuge system.

This study aims to map the confidence interval associated with capillary pressure data and average sample saturation as monitored by different centrifuge configurations and automated high resolution cameras to monitor the fluid production.

2 Fundamentals for Centrifuge Method

Capillary pressure (Pc) in a porous medium containing oil and water is defined as the pressure in the oil phase (Po) minus the pressure in the aqueous phase (Pw). In terms of fluid height (h) above the level of free water, it can be expressed as follows:

$$Pc = (\Delta\rho)gh \tag{1}$$

where (g) is the gravity and $(\Delta\rho)$ is the difference between oil density (ρ_o) and water phase density (ρ_w).

The Young-Laplace equation describes the pressure difference across the interface between two static fluids as:

$$Pc = \sigma\left(\frac{1}{R_1} + \frac{1}{R_2}\right) \tag{1}$$

where σ is the interfacial tension and R_1 and R_2 are the principal radii of curvature of the interface.

In 1945, Hassler and Brunner proposed a novel method for obtaining capillary pressure curves [12]. They suggested centrifuging the core sample, allowing for the complete range of saturations required by the sample properties, along with the radially varying centrifugal force within the sample. The raw data obtained from the centrifuge test requires a transformation based on assumptions regarding the physics of fluid displacement. In this case, the acceleration due to gravity is given by:

$$g = \omega^2.r \tag{2}$$

Where r is the radius from the center of rotation to any point along the length of the rock sample length (L) in cm, and ω is the angular velocity given by:

$$\omega = \frac{2\pi N}{60}\left(\frac{rad}{seg}\right) \tag{3}$$

where N is the speed of the centrifuge in revolutions per minute (rpm).

Inserting equation (2) into equation (1) and expressing it in the differential form:

$$dPc = -(\Delta\rho)\,(\omega^2.r)\,(dr) \tag{4}$$

Integrating the equation (4) between the distances from the rotation axis to the inlet end face (r_1) and to the outlet end face (r_2) of the core for a constant speed (ω) as follows,

$$Pc_1 - Pc_2 = -\frac{1}{2}\Delta\rho\omega^2({r_1}^2 - {r_2}^2) \tag{5}$$

The water saturation varies along the length of the core, ranging from near zero at the inlet end face (S_{w1}), where the capillary pressure is maximum (Pc_1), to a maximum water saturation of 100% at the outlet end face (S_{w2}), where the capillary pressure is zero $(Pc_2 = 0)$. Therefore, Eq. 5 can be rewritten as:

$$Pc_1 = \frac{1}{2}\Delta\rho\omega^2({r_2}^2 - {r_1}^2) \tag{6}$$

The capillary pressure distribution is linked to a fluid saturation distribution along the length of the core. During the centrifuge tests, the average saturation of the sample is determined by monitoring the fluid production from the sample. The initial assumption is that hydrostatic equilibrium is indeed attained for each measurement step. The average saturation of the sample at each rotation $(\bar{S}_N)$ is given by the ratio between the produced volume (V_N) and the pore volume (V_p).

$$\bar{S}_N = \frac{V_N}{Vp} \tag{7}$$

The produced effluent volume reflects the average fluid saturation in the core, rather than the actual saturation variation across the core. In order to construct the capillary pressure curve for the sample, the centrifuge method requires the use of analytical and/or numerical techniques to relate the average saturation $(\bar{S}_N)$ to the inlet saturation (S_{w1}^N), as the measured capillary pressure corresponds to the inlet face of the core (Pc_1^N).

Therefore, the centrifuge technique involves two main experimental steps: measuring the centrifuge speed (N) and the fluid production (V_N) data. The other parameters are imposed by the centrifuge model design and the porous samples used.

The efficiency and accuracy of centrifuge measurements depend significantly on the equipment design and the method used to monitor the volume of fluid displaced at each rotation speed typically through optical systems or manual observation.

Ferno et al. [9] reported that produced volume measurements based on visual techniques have limited precision, with a volumetric accuracy of approximately 0.1 cm^3 at best, resulting in a saturation uncertainty of about 0.006 PV for a 15 cm^3 pore volume. It is important

to note that this estimate accounts only for the uncertainty associated to the produced volume measurement.

Automated systems including cameras allow for accuracy of produced fluid volumes of better than 0.05 cc [20]. According to Ferno et al. [9], a high degree of automation and precise imaging systems in centrifuge setups significantly improves the reliability of production measurements by eliminating bias and enabling the detection of very small volume changes (~0.01 cc). The use of fixed cameras significantly reduces the risk of parallax error; however, it does not eliminate it entirely, as the fluid meniscus may shift during the experiment while the camera position remains unchanged. Despite this limitation, the enhanced precision of the system substantially minimizes parallax effects in such setup.

3 Uncertainty Analysis

As pointed before, the results are fully dependent on the rock sample properties, displaced and displacing fluid properties and the centrifuge characteristics. Experimental data acquisitions include uncertainties correlated with instruments resolutions used to measured variables. Those uncertainties can be propagated to the calculated variables according to their modelling, conferring a reliability range to the obtained results. See the general following derivation.

The absolute uncertainty of a result $R(x, y, z)$, which is a function of several independent variables x, y, z is given by Eq. 8 [21].

$$\omega_R^2 = \left(\frac{\partial \omega_R}{\partial x}\right)^2 \omega_x^2 + \left(\frac{\partial \omega_R}{\partial y}\right)^2 \omega_y^2 + \left(\frac{\partial \omega_R}{\partial z}\right)^2 \omega_z^2 + \cdots \quad (8)$$

Where ω_R is the uncertainty on the calculated result, $\omega_x, \omega_y, \omega_z$ are the uncertainties of the measured variables, and the terms $\partial\omega_R/\partial x$, $\partial\omega_R/\partial y$, $\partial\omega_R/\partial z$ correspond to the partial derivatives of the function $R(x, y, z)$ with respect to the variables x, y, z, respectively.

The uncertainty on the result can also be expressed in a relative way [21], as

$$\frac{\omega_R}{R} = \left[\left(\frac{1}{R}\frac{\partial \omega_R}{\partial x}\right)^2 \omega_x^2 + \left(\frac{1}{R}\frac{\partial \omega_R}{\partial y}\right)^2 \omega_y^2 \left(\frac{1}{R}\frac{\partial \omega_R}{\partial z}\right)^2 \omega_z^2\right]^{1/2} \quad (9)$$

Particular derivations for the centrifuge data obtained are presented in Table 1.

Although much of the robustness of the centrifuge method relies on the data processing step, particularly in estimating inlet face saturation, this study focuses solely on the uncertainties associated with experimental variables. We do not address uncertainties related to the analytical models for determining boundary saturations, nor temperature effects on fluid properties, test repeatability, operator-dependent, camera-induced parallax errors, or other unforeseen factors. Instead, we isolate and quantify the uncertainties propagated from equipment and sample parameters, providing an integrated view of the instrumentation impact on capillary pressure measurements.

Table 1. Equations and relative uncertainties of calculated variables.

Area open to the flow and relative uncertainty	$A = \pi\left(\frac{D}{2}\right)^2$	$\frac{\omega_A}{A} = \sqrt{\left(\frac{2\omega_D}{D}\right)^2}$
Total volume	$V_T = A.L$	$\frac{\omega_V}{V_T} = \sqrt{\left(\frac{\omega_A}{A}\right)^2 + \left(\frac{\omega_L}{L}\right)^2}$
Pore volume (gravimetric)	$V_p = \frac{m_{sat} - m_{dry}}{\rho_w}$	$\frac{\omega_{Vp}}{V_p} = \sqrt{\left(\frac{\omega_{m_{sat}}}{\Delta m}\right)^2 + \left(\frac{\omega_{m_{dry}}}{\Delta m}\right)^2 + \left(\frac{\omega_{\rho_w}}{\rho_w}\right)^2}$
Porosity	$\phi = \frac{V_P}{V_T}$	$\frac{\omega_\phi}{\phi} = \sqrt{\left(\frac{\omega_{V_P}}{V_P}\right)^2 + \left(\frac{\omega_{V_T}}{V_T}\right)^2}$
Water to oil density	$\Delta\rho = \rho_w - \rho_o$	$\frac{\omega_{\Delta\rho}}{\Delta\rho} = \sqrt{\left(\frac{\omega_{\rho_o}}{\Delta\rho}\right)^2 + \left(\frac{\omega_{\rho_w}}{\Delta\rho}\right)^2}$
Capillary pressure at the outlet	$Pc_1 = \frac{1}{2}\Delta\rho\omega^2(r_2{}^2 - r_1{}^2)$	
	$\frac{\omega Pc}{Pc} = \sqrt{\left(\frac{\omega\rho_w}{\Delta\rho}\right)^2 + \left(\frac{\omega\rho_o}{\Delta\rho}\right)^2 + \left(\frac{2\omega_\omega}{\omega}\right)^2 + \left(\frac{2r_1\omega_{r1}}{r_2{}^2 - r_1{}^2}\right)^2 + \left(\frac{2r_2\omega_{r_2}}{r_2{}^2 - r_1{}^2}\right)^2}$	
Average sample water saturation	$\bar{S}_w = \frac{V_P - V_{Prod}}{V_P}$	$\frac{\omega_{\bar{S}_w}}{\bar{S}_w} = \sqrt{\left(\frac{\omega_{V_P}}{\Delta V}\right)^2 + \left(\frac{\omega_{V_{Prod}}}{\Delta V}\right)^2 + \left(\frac{\omega_{V_P}}{V_P}\right)^2}$

4 Materials and Methods

4.1 Centrifuges Equipment

The sensitivity analysis presented in this study was conducted using four centrifuge models, each exhibiting distinct characteristics, including variations in produced volume resolution, drainage and imbibition arm lengths, maximum operational speeds, and maximum allowable sample lengths. Technical specifications for each centrifuge were obtained from the manufacturer's manuals. To maintain confidentiality, the centrifuge models are designated as A, B, C, and D.

Centrifuge D features the largest drainage and imbibition radii, followed by Centrifuge A, and Centrifuges C and B. Centrifuge B supports the highest maximum speed, whereas, those centrifuges having larger radii exhibit lower maximum speeds, which reflects the typical trade-off between the radius and rotational speed in achieving a given capillary pressure. The camera resolution for the volume measurement was given for each centrifuge according to the sample cup's max volume. The main characteristics of each device are summarized in Table 1. All the centrifuge characteristics were incorporated into the uncertainty propagation calculations of the measured results.

Table 2. Centrifuge Properties.

	Centrifuge Properties	Symbol	Unit	Value	Resolution/Uncertainty
A	Speed Range_ Drainage	ω	rpm	300 – 8,000	3 – 80 (1)
	Speed Range _ Imbibition	ω	rpm	300 – 8,000	3 – 80 (1)
	Arm of the centrifuge - Drainage	r_2	cm	12.32	0.01 (2)
	Arm of the centrifuge - Imbibition	r_2	cm	19.37	0.01 (2)
	Sample diameter	d	cm	3.81	0.01 (2)
	Max Sample size	L	cm	7.62	0.01 (2)
	Sample Cup Max Volume	V_{Nmax}	cm^3	25	0.1 (3)
B	Speed Range _ Drainage	ω	Rpm	Up to 16,500	Up to 165 (1)
	Speed Range _ Imbibition	ω	rpm	Up to 15,000	Up to 150 (1)
	Arm of the centrifuge - Drainage	r_2	cm	9.13	0.01(2)
	Arm of the centrifuge - Imbibition	r_2	cm	16.63	0.01(2)
	Max Sample Diameter	d	cm	3.950	0.001(2)
	Max Sample size	L	cm	5.207	0.001(2)
	Sample Cup Max Volume	V_{Nmax}	cm^3	3, 6, 12 and 23	0.003 – 0.084(3)
C	Speed Range _ Drainage	ω	rpm	300 – 10,000	3 - 100
	Speed Range _ Imbibition	ω	rpm	300 – 10,000	3 - 100
	Arm of the centrifuge - Drainage	r_2	cm	9.20	0.01(2)
	Arm of the centrifuge - Imbibition	r_2	cm	16.47	0.01(2)
	Sample diameter	d	cm	3.81	0.01(2)
	Max Sample size	L	cm	5.50	0.01(2)
	Sample Cup Max Volume	V_{Nmax}	cm^3	21	0.025(3)
D	Speed Range _ Drainage	ω	rpm	200 – 4,500	2 - 45
	Speed Range _ Imbibition	ω	rpm	200 – 4,500	2 - 45
	Arm of the centrifuge - Drainage	r_2	cm	21.55	0.01 (2)
	Arm of the centrifuge - Imbibition	r_2	cm	25.60	0.01 (2)
	Sample diameter	d	cm	3.81	0.01(2)
	Max Sample size	L	cm	10.16	0.01(2)
	Sample Cup Max Volume	V_{Nmax}	cm^3	10 and 32	0.01 (2)

(1) 1% of the full scale range; (2) Fluctuation of least significant digit informed in the equipment manual; (3) Camera resolution

4.2 Rock Samples and Fluids

Three sandstone outcrop samples were selected for this study, samples A1, A2 and A3. Prior to testing, samples were fully saturated with a synthetic brine solution, that was prepared to replicate the formation water (FW) composition, corresponding to NaCl at 207 kppm. A mineral oil was used as an oleic phase. The porous samples dimensions were measured using a precision caliper and its permeability was determined using a Core Lab Gas Permeameter and employing nitrogen (N_2) as the flowing fluid. The pore volume of each sample was calculated based on the mass difference between dry and fully saturated samples, and the density of the fluids. The mass measurements were performed using an analytical scale and the fluids density using a Densitometer Anton Paar DMA™ 5000 M. The instruments used to measure the samples properties are listed in Table 3 and the obtained properties of the cleaned samples, including the corresponding uncertainties, are summarized in Table 4.

Subsequent centrifugation experiments were conducted exclusively using Centrifuge B. The experiments were conducted using 23 mL collection cups and a dead volume of 2.5 mL of brine. These tests aimed to generate capillary pressure data, which were then analyzed to evaluate measurement accuracy and the uncertainties propagation of the experimental procedures.

Table 3. Rock and fluid measured parameters, instruments used and the corresponding resolution.

Rock sample properties	**Symbol**	**Unit**	**Instrument**	**Resolution**
Sample diameter	D	cm	Caliper	0.005
Sample length	L	cm	Caliper	0.005
Dry mass	m_{dry}	g	Analytical Scale	0.001
Fully saturated mass	m_{sat}	g	Analytical Scale	0.001
Fluid properties	**Symbol**	**Unit**	**Instrument**	**Resolution**
Oil density	ρ_o	g/cm^3	Densimeter	0.0005
Water density	ρ_w	g/cm^3	Densimeter	0.00001

Table 4. Rock Sample and Fluid Properties for the Study Cases.

Rock sample properties	**Sample A1**	**Sample A2**	**Sample A3**
D [cm]	3.795 ± 0.005	3.784 ± 0.005	3.784 ± 0.005
L [cm]	4.976 ± 0.005	4.965 ± 0.005	4.965 ± 0.005
m_{dry} [g]	109.602 ± 0.001	109.259 ± 0.001	109.747 ± 0.001
m_{sat} [g]	125.455 ± 0.001	125.031 ± 0.001	125.590 ± 0.001
V_P [cm^3]	13.963 ± 0.001	13.892 ± 0.001	13.955 ± 0.001
ϕ [%]	24.81 ± 0,07	24.88 ± 0.07	24.99 ± 0.07
k [mD]	169.4 ± 0.5	179.6 ± 0.5	153.7 ± 0.5
Fluid properties			
ρ_o [g/cm^3]	0.8417 ± 0.0005		
ρ_w [g/cm^3]	1.13531 ± 0.00001		

5 Results

Based on the specifications provided in the equipment manuals (Table 2), the minimum and maximum capillary pressures attainable by each centrifuge during the drainage and imbibition processes were calculated (Eq. 6 or Table 1). The results for the tested rocks summarized in Table 5 were obtained taking into account the maximum allowable sample length and the centrifuge speed range for each device. For longer core samples, higher capillary pressures are observed at the sample face under the same rotational speed ($P_{c,\omega=1000}$), as shown in Table 5. Achieving a specific capillary pressure requires a lower centrifuge rotational speed for longer samples, due to the high radial distance contributing to the pressure gradient. Centrifuge B reaches the highest capillary pressures. As the lowest value, the manual indicates 1000 rpm as the minimum safe rotational speed for this centrifuge. That feature may influence the initial portion of the capillary pressure curves, particularly in samples with larger pore sizes. Inversely, centrifuges with lower maximum capillary pressure capacities may be unable to generate sufficient pressure for tight samples to reach irreducible water saturation.

The same calculations were performed considering samples 5 cm long and tested in the four centrifuge models (Table 6).

Table 5. Capillary pressure range for drainage and imbibition, based on the maximum sample length allowed in each device.

Centrifuge	**A**	**B**	**C**	**D**
Drainage				
$P_{c,min}$ [psi]	0.27 ± 0.01	-	0.15 ±0.0	0.31 ±0.01
$P_{c,\omega=1000}$ [psi]	3.03 ± 0.06	1.59 ± 0.03	1.66 ± 0.03	7.81 ± 0.16
$P_{c,max}$ [psi]	193.8 ± 3,9	432.1 ± 9.1	165.7± 3.5	158.2 ± 3.2
Imbibition				
$P_{c,min}$ [psi]	0.50 ± 0.01	-	0.32 ± 0.01	0.39 ± 0.01
$P_{c,\omega=1000}$ [psi]	5.54 ± 0.11	3.41 ± 0.07	3.52 ± 0.07	9.74 ± 0.2
$P_{c,max}$ [psi]	354.4 ± 7.2	767.4 ± 15.7	352.4 ± 7.2	197.2 ± 4.0

Table 6. Capillary pressure range for drainage and imbibition processes considering a sample with a length of 5 cm.

Centrifuge	**A**	**B**	**C**	**D**
Drainage				
$P_{c,min}$ [psi]	0.21 ± 0.00	-	0.14 ± 0.00	0.18 ± 0.00
$P_{c,\omega=1000}$ [psi]	2.29± 0.05	1.55 ± 0.03	1.56 ± 0.03	4.45 ± 0.09
$P_{c,max}$ [psi]	146.8 ±3.0	421.5 ± 8.9	156.4 ± 3.3	90.1 ± 1.8

Imbibition				
$P_{c,min}$ [psi]	0.35 ± 0.01	-	0.29 ± 0.02	0.22 ± 0.00
$P_{c,\omega=1000}$ [psi]	3.94 ± 0.08	3.30 ± 0.07	3.26 ± 0.07	5.39 ± 0.11
$P_{c,max}$ [psi]	252.1 ± 5.0	742.4 ± 15.2	326.2 ± 6.7	109.2 ± 2.2

A comparison of the results for shorter samples, such as that 5 cm in length, reveals a further reduction in the maximum capillary pressure achieved by Centrifuge D. As shown in Tables 5 and 6, the maximum capillary pressure decreases from approximately 160 psi during drainage and 200 psi during imbibition for longer samples to 90 psi during drainage and 109 psi during imbibition for shorter samples (5 cm in length). However, Centrifuge D is the only centrifuge allowing longer samples, with lengths up to 10cm. Longer samples can be considered more representative of reservoir conditions in capillary pressure experiments, as the increased rock volume provides a more realistic approximation of fluid distribution and pore-scale heterogeneity. On the other hand, it is common practice to use reservoir core plugs with lengths around 5 cm, which aligns with standard sample dimensions widely adopted in core analysis laboratories.

In addition, Tables 5 and 6 indicate that the relativity uncertainty associated with capillary pressure is around 2%.

In order to investigate how uncertainty magnitude changes across the capillary pressure curve, a study case was conducted. Sandstone outcrop samples fully saturated with brine were centrifuged with mineral oil using centrifuge B. The Δρ between water and oil was the same as in Table 4.

The capillary pressure versus average water saturation curve of sample A2 (randomly selected) was used as a reference to extrapolate expected fluid production for the other centrifuges. While experimental data were obtained exclusively from Centrifuge B, the water production for Centrifuges A, C, and D was estimated using a linear interpolation approach based on the *Pc–Sw* relationship observed in Centrifuge B. The maximum produced volume was limited by the maximum volume obtained in the test for the sample using Centrifuge B. Also, the maximum speed of each centrifuge was respected. Table 7 shows the experimental data and corresponding uncertainties for sample A2, using the Centrifuge B. Assuming the same rotational speeds as Centrifuge B, the capillary pressures, for the estimated production data, and the corresponding uncertainties were obtained for Centrifuges A, C, and D (see Tables 8, 9 and 10 respectively).

The absolute uncertainties in the capillary pressure values demonstrate the proportionality between the measurement error and the magnitude of Pc for all the equipment. In other words, the uncertainties are proportional to the measured variable, maintaining a constant ratio between the uncertainty and the capillary pressure value. This behavior is justified since one of the highest uncertainty contributions is related to the rotational speed uncertainty, assumed to be around 1%.

When comparing the saturation results using the same rock sample across all devices, the relative uncertainties observed were 0.0102 for Centrifuge A, 0.0086 for Centrifuge B, 0.0025 for Centrifuge C, and 0.0010 for Centrifuge D. These differences are directly influenced by each centrifuge's volume measurement resolution. The strong correlation between resolution and measurement uncertainty emphasizes the importance of high-precision systems for minimizing experimental errors. Centrifuge D demonstrates superior performance in reducing uncertainty, primarily due to its fine volume resolution and extended arm radius, which enhance both sensitivity and capillary pressure gradient definition during centrifugation. However, Centrifuge D has the lowest maximum rotational speed (4500 RPM) among the evaluated centrifuges, which may be insufficient to generate the capillary pressure required to reach the irreducible water saturation, especially in small samples. This limitation was evident in the present study: while Centrifuges A, B, and C reached a final water saturation of 16.05%, Centrifuge D reached only 19.05%, indicating incomplete desaturation under equivalent operating conditions.

Table 7. Data and respective uncertainty resulting from Drainage Calculated to Centrifuge A using Sample A2.

Speed [rpm]	Produced Volume (cc)	Pc in the inlet face (psi)	ω_{Pc} (psi)	Uncertainty of Pc (%)	$\overline{Sw}$ (frac)	$\omega_{\overline{Sw}}$ (frac)	Uncertainty of $\overline{Sw}$ (%)
1300	7.0	3.85	0.08	2.1	0.4933	0.0102	2.1
1600	8.1	5.84	0.12	2.0	0.4135	0.0102	2.5
1900	8.9	8.23	0.17	2.0	0.3603	0.0102	2.8
2200	9.4	11.04	0.22	2.0	0.3259	0.0102	3.1
2500	9.7	14.26	0.29	2.0	0.3001	0.0102	3.4
3000	10.1	20.53	0.42	2.0	0.2756	0.0102	3.7
4000	10.6	36.50	0.74	2.0	0.2369	0.0102	4.3
5000	10.9	57.02	1.16	2.0	0.2155	0.0102	4.7
7000	11.5	111.8	2.3	2.0	0.1730	0.0102	5.9
8000	11.7	146.0	3.0	2.0	0.1605	0.0102	6.3

Table 8. Data and respective uncertainty resulting from Drainage Test on Centrifuge B using Sample A2 and 23cm^3 cup.

Speed [rpm]	Produced Volume (cc)	Pc in the inlet face (psi)	ω_{Pc} (psi)	Uncertainty of Pc (%)	$\overline{Sw}$ (frac)	$\omega_{\overline{Sw}}$ (frac)	Uncertainty of $\overline{Sw}$ (%)
1300	5.783	2.60	0.06	2.1	0.5837	0.0086	1.5
1600	7.130	3.95	0.08	2.1	0.4867	0.0086	1.8
1900	8.051	5.56	0.12	2.1	0.4205	0.0086	2.0
2200	8.716	7.46	0.16	2.1	0.3726	0.0086	2.3
2500	9.196	9.63	0.20	2.1	0.3380	0.0086	2.5
3000	9.702	13.87	0.29	2.1	0.3016	0.0086	2.8
4000	10.288	24.66	0.52	2.1	0.2595	0.0086	3.3
5000	10.655	38.53	0.81	2.1	0.2330	0.0086	3.7
7000	11.141	75.52	1.59	2.1	0.1980	0.0086	4.3
8000	11.314	98.64	2.08	2.1	0.1856	0.0086	4.6
9000	11.663	124.85	2.64	2.1	0.1605	0.0086	5.3

Table 9. Data and respective uncertainty resulting from Drainage Test Calculated to Centrifuge C using Sample A2.

Speed [rpm]	Produced Volume (cc)	Pc in the inlet face (psi)	ω_{Pc} (psi)	Uncertainty of Pc (%)	$\overline{Sw}$ (frac)	$\omega_{\overline{Sw}}$ (frac)	Uncertainty of $\overline{Sw}$ (%)
1300	5.811	2,63	0,06	2,1	0,5817	0,0025	0,4
1600	7.154	3.99	0.08	2.1	0.4850	0.0025	0.5
1900	8.072	5.62	0.12	2.1	0.4190	0.0025	0.6
2200	8.734	7.54	0.16	2.1	0.3713	0.0025	0.7
2500	9.209	9.73	0.21	2.1	0.3371	0.0025	0.8
3000	9.710	14.02	0.30	2.1	0.3011	0.0025	0.8
4000	10.295	24.92	0.53	2.1	0.2590	0.0025	1.0
5000	10.660	38.94	0.82	2.1	0.2327	0.0025	1.1
7000	11.147	76.32	1.18	2.1	0.1976	0.0025	1.3
8000	11.328	99.68	2.10	2.1	0.1846	0.0025	1.4
9000	11.663	126.16	2.66	2.1	0.1605	0.0025	1.6

Table 10. Data and respective uncertainty resulting from Drainage Test Calculated to Centrifuge D using Sample A2.

Speed [rpm]	Produced Volume (cc)	Pc in the inlet face (psi)	ω_{Pc} (psi)	Uncertainty of Pc (%)	$\overline{Sw}$ (frac)	$\omega_{\overline{Sw}}$ (frac)	Uncertainty of $\overline{Sw}$ (%)
1300	8.719	7.47	0.15	2.0	0.3724	0.0010	0.3
1600	9.397	11.32	0.23	2.0	0.3236	0.0010	0.3
1900	9.815	15.96	0.33	2.0	0.2935	0.0010	0.3
2200	10.110	21.40	0.44	2.0	0.2722	0.0010	0.4
2500	10.366	27.63	0.56	2.0	0.2538	0.0010	0.4
3000	10.671	39.79	0.81	2.0	0.2319	0.0010	0.4
4000	11.078	70.74	1.44	2.0	0.2026	0.0010	0.5
4500	11.246	89.53	1.82	2.0	0.1905	0.0010	0.6

Figure 3 presents the capillary pressure curves as a function of average saturation for the different centrifuge devices evaluated in this study (results from Tables 7 to 10). The nominal uncertainties were included in each point. The shape of the curve is consistent with typical drainage behavior in porous media. Centrifuges A, B, and C show good agreement with each other throughout the curves, with a clear overlap of points and relatively small error bars. Although Centrifuge D offers superior precision, as evidenced by the smallest uncertainty bars, its limited operational speed constrains its ability to reach higher capillary pressures, resulting in incomplete desaturation (see also Table 10). In contrast, Centrifuges A, B, and C reach similar saturation levels with higher associated uncertainties, highlighting a trade-off between operational range and measurement precision (see Table 7, 8 and 9).

The plot reveals that the uncertainty in capillary pressure increases with the magnitude of Pc. This behavior aligns with the propagation of rotational speed errors, which become more significant at higher angular velocities due to the quadratic relationship between Pc and rotational speed. Uncertainties at low saturations (i.e., high Pc values) are particularly critical, as this region is essential for determining irreducible water saturation and relative permeability functions. The larger vertical error bars in this range highlight the importance of using high-resolution sensors and maintaining stable rotational systems to

ensure accurate capillary pressure curve estimation. Overall, incorporating Pc uncertainties enhances the comparison between devices and underscores the necessity of optimizing measurement systems in centrifuge-based experiments, especially when operating at elevated pressures.

Two additional samples of the same outcrop were tested using centrifuge B. The centrifuge data are shown in Tables 11 and 12, and the capillary pressure versus saturation curves are shown in Figure 4.

The capillary pressure profiles of the three evaluated sandstone samples reveal a remarkably consistent behavior. A substantial desaturation is observed at the first measurement point, suggesting that the test should have been initiated at a lower rotational speed to capture the initial, gradual desaturation process more accurately. This underscores the necessity for centrifuge systems to operate at reduced speeds, ideally below 1000 RPM, to enable high-resolution observation of early saturation changes. Following the initial point, the curves exhibit a smooth desaturation trend, indicative of a uniform distribution of pore throat sizes an expected feature of well-sorted sandstone formations.

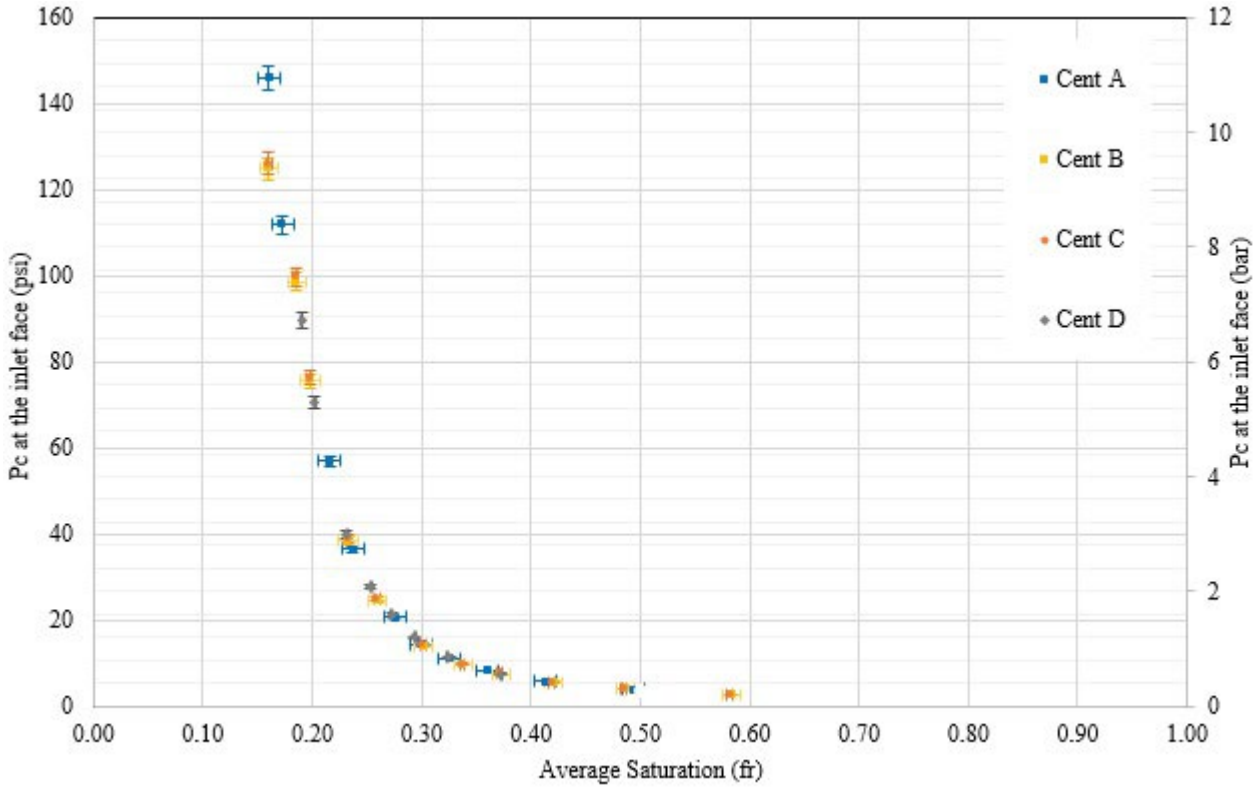

Fig 3. Comparison of capillary pressure vs. average saturation obtained from centrifuges A, B, C, and D with associated uncertainties.

Table 11. Data and respective uncertainty resulting from Drainage Test on Centrifuge B using Sample A1.

Speed [rpm]	Produced Volume (cc)	Pc in the inlet face (psi)	ω_{Pc} (psi)	Uncertainty of Pc (%)	$\overline{Sw}$ (frac)	$\omega_{\overline{Sw}}$ (frac)	Uncertainty of $\overline{Sw}$ (%)
1300	5.597-	2.61	0.06	2.1	0.5991	0.0085	1.4
1600	7.083	3.95	0.08	2.1	0.4928	0.0085	1.7
1900	7.947	5.57	0.12	2.1	0.4309	0.0085	2.0
2200	8.580	7.47	0.16	2.1	0.3856	0.0085	2.2
2500	9.081	9.65	0.20	2.1	0.3497	0.0085	2.4
3000	9.630	13.89	0.29	2.1	0.3103	0.0085	2.7
4000	10.240	24.70	0.52	2.1	0.2667	0.0085	3.2
5000	10.605	38.59	0.81	2.1	0.2405	0.0085	3.5
7000	11.102	75.63	1.60	2.1	0.2049	0.0085	4.2
8000	11.292	98.78	2.09	2.1	0.1913	0.0085	4.4
9000	11.632	125.02	2.64	2.1	0.1670	0.0085	5.1

Table 12. Data and respective uncertainty resulting from Drainage Test on Centrifuge B using Sample A3.

Speed [rpm]	Produced Volume (cc)	Pc in the inlet face (psi)	ω_{Pc} (psi)	Uncertainty of Pc (%)	$\overline{Sw}$ (frac)	$\omega_{\overline{Sw}}$ (frac)	Uncertainty of $\overline{Sw}$ (%)
1300	5.7332	2.60	0.06	2.5	0.5892	0.0085	1.4
1600	7.2738	3.94	0.10	2.5	0.4788	0.0085	1.8
1900	8.1908	5.56	0.14	2.5	0.4131	0.0085	2.1
2200	8.8292	7.46	0.19	2.5	0.3673	0.0085	2.3
2500	9.3248	9.63	0.24	2.5	0.3318	0.0085	2.6
3000	9.8306	13.86	0.35	2.5	0.2956	0.0085	2.9
4000	10.4310	24.65	0.61	2.5	0.2525	0.0085	3.4
5000	10.8166	38.51	0.96	2.5	0.2249	0.0085	3.8
7000	11.3040	75.48	1.88	2.5	0.1900	0.0085	4.5
8000	11.4850	98.58	2.45	2.5	0.1770	0.0085	4.8
9000	11.8308	124.77	3.11	2.5	0.1522	0.0085	5.6

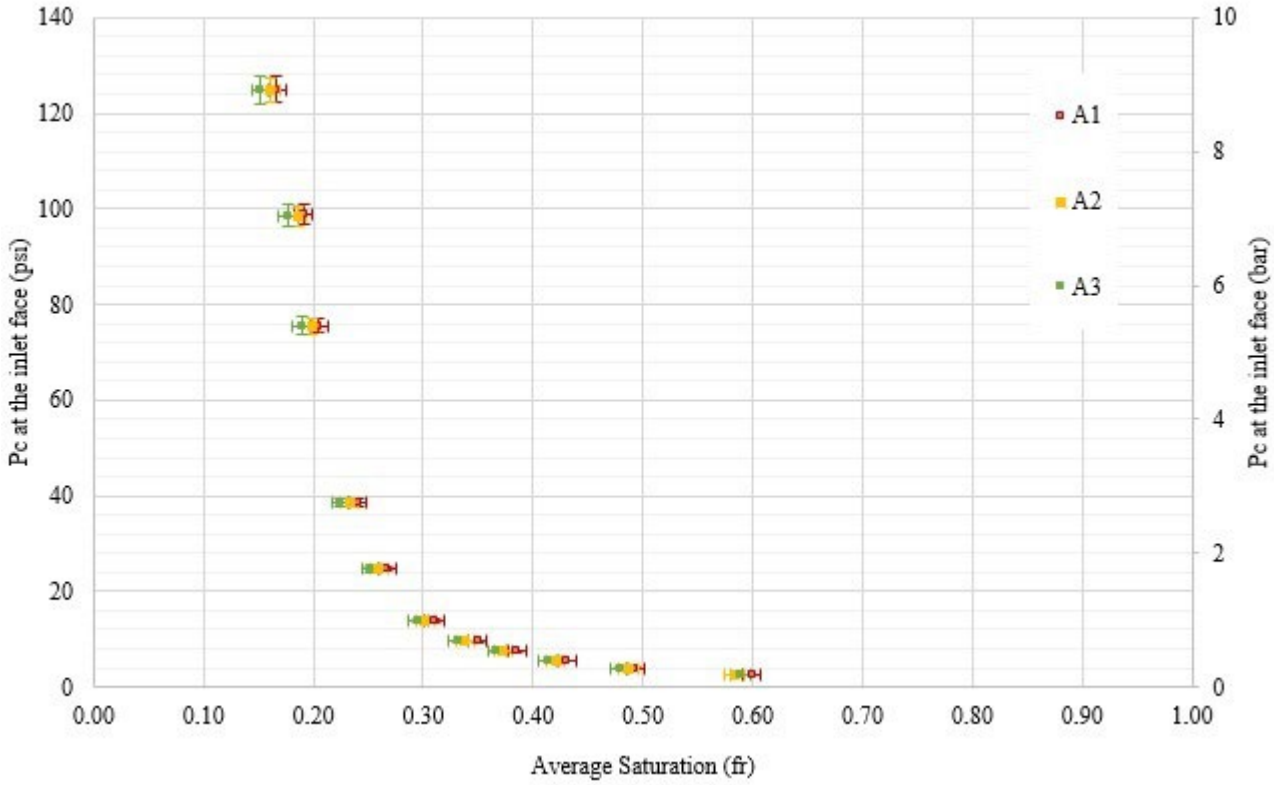

Fig 4. Capillary pressure vs. average saturation for sandstones outcrop samples A1, A2 and A3.

At higher rotational speeds, a slight deviation in curve slope is detected, which may be attributed either to intrinsic sample characteristics or insufficient equilibration time at each centrifugal step. All three samples reached a final irreducible water saturation of approximately 16%.

It is also noteworthy to highlight that for lithology-similar samples, such as the evaluated sandstones, the uncertainty magnitude remains relatively uniform. However, in the case of more heterogeneous rock types, particularly carbonates, the uncertainties could considerably increase. This variability may directly affect the fidelity of capillary pressure data used in reservoir simulation workflows, highlighting the need for rigorous error assessment in such studies.

6 Conclusions

This study assessed the influence of centrifuge specifications (namely rotational speed, measurement resolution, and allowable sample length) on the accuracy and propagated uncertainty of capillary pressure data. The analysis confirmed that device characteristics significantly affect the reliability of experimental results. High-resolution cameras and larger arm radii contributed to reduced uncertainty levels, while limitations in maximum rotational speed constrained the achievable capillary pressure range. Among the centrifuges evaluated, Centrifuge D yielded the lowest relative uncertainty, although it did not reach the same irreducible water saturation as the other devices due to speed limitations.

The uncertainty analysis showed that relative uncertainty in saturation increases with capillary pressure. Including uncertainty bars in capillary pressure curves is especially important in reservoir studies involving heterogeneous sample sets, where significant variability may occur at a given pressure level. This graphical representation enhances interpretation and supports a more robust integration of experimental data into reservoir models.

Furthermore, the precision of equipment used during sample preparation plays a non-negligible role in the final uncertainty. Careful handling, consistent methodologies, and adherence to laboratory best practices are essential to ensure the repeatability and accuracy of centrifuge-based experiments.

Overall, the findings provide a quantitative foundation for selecting and optimizing centrifuge systems and associated experimental procedures. By accounting for equipment-induced uncertainties, this study contributes to improved capillary pressure data reliability, supporting more accurate special core analysis.

We gratefully acknowledge the support and sponsorship by Petrobras (Projects ANP 23557-2 and 23486-4). We also acknowledge the support of ANP (Brazil's National Oil, Natural Gas and Biofuels Agency) through the R&D levy as well as the valuable contributions of the Labore Research Group to this study.

References

1. Aghaeifar Z., Strand S., and Puntervold T. Significance of Capillary Forces during Low-Rate Waterflooding Energy & Fuels 33 (5), 3989-3997 (2019): https://pubs.acs.org/doi/10.1021/acs.energyfuels.9b00023
2. Masalmeh S. K.; Jing X. D. Capillary Pressure Characteristics of Carbonate Reservoirs: Relationship Between Drainage and Imbibition Curves. International Symposium of the Society of Core Analysts. Trondheim, Norway (2006).
3. Golaz, P., and A.G. Bentsen. On the Use of the Centrifuge to Obtain Capillary Pressure Data. Annual Technical Meeting, Calgary, Alberta (1980): https://doi.org/10.2118/80-31-38
4. Shikhov I.; Arns, C.H. Evaluation of Capillary Pressure Methods via Digital Rock Simulations. Transp Porous Med 107, 623–640 (2015): https://doi.org/10.1007/s11242-015-0459-z
5. McPhee C. Reed J., Zubizarreta Z. Chapter 9 - Capillary Pressure. Developments in Petroleum Science 64, 449 – 517 (2015): https://doi.org/10.1016/B978-0-444-63533-4.00009-3
6. Melrose, J. C.; Dixon, J. R.; Mallinson, J. E. Comparison of Different Techniques for Obtaining Capillary Pressure Data in the Low-Saturation Region. SPE Form Eval 9, 185–192 (1994): https://doi.org/10.2118/22690-PA
7. Jiao, Y.; Li, X.; Wang, Y. Applications of mercury intrusion capillary pressure for pore structures: A review. Capillarity, 3(4), 62–74 (2020): https://www.sciopen.com/article/pdf/10.46690/capi.2020.04.02.pdf?ifPreview=0
8. Lenormand, R. Capillary pressure and pore size distribution from water injection: A feasibility study. Society of Core Analysts. SCA2012-41 (2012): https://www.jgmaas.com/SCA/2012/SCA2012-41.pdf
9. Fernø, M.A.; Treinen, R.; Graue, A. Experimental Measurement of Capillary Pressure with the Centrifuge Technique – Emphasis on Equilibrium Time and Accuracy in Production - International Symposium of the Society of Core Analysts Calgary, Canada, (2007): https://jgmaas.com/SCA/2007/SCA2007_22.pdf
10. Badawy A. M. Ganat T. A. A. O. *Rock Properties and Reservoir Engineering: A Practical View Petroleum Engineering* ISBN 978-3-030-87462-9 (eBook) Springer Nature Switzerland AG (2022): https://doi.org/10.1007/978-3-030-87462-9
11. Christiansen, R. L. Geometric Concerns for Accurate Measurement of Capillary Pressure Relationships with Centrifuge Methods. SPE Form Eval 7 (04): 311–314 (1992): https://doi.org/10.2118/19026-PA
12. Hassler, G.L.; Brunner, E. Measurement of Capillary Pressures in Small Core Samples. Trans. 160 (1945): 114–123: https://doi.org/10.2118/945114-G

13. Rajan, R.R. Theoretically Correct Analytical Solution for Calculating Capillary Pressure-Saturation from Centrifuge Experiments. SPWLA 27th Annual Logging Symposium, Houston, Texas, (1986).
14. Skuse, B.; Flroozabadi, A.; Ramey H. J. Computation and Interpretation of Capillary Pressure from a Centrifuge. SPE Form Eval 7 17–24. (1992): https://doi.org/10.2118/18297-PA
15. Forbes, P. Simple and Accurate Methods for Converting Centrifuge Data into Drainage and Imbibition Capillary Pressure Curves. *The Log Analyst* 35 (1994)
16. Forbes P.; Chen Z. A.; Ruth D. W. Quantitative Analysis of Radial Effects on Centrifuge Capillary Pressure Curves 69th Annual Technical Conference ana Exhibition, New Orleans, LA, USA (1994).
17. Chen, Z. A.; Ruth D. W. Measurement and Interpretation of Centrifuge Capillary Pressure Curves-the Sca Survey Data. The Log Analyst 36 (1995).
18. Moghaddam, R. N. A Rapid and Accurate Method for Calculation of Capillary Pressure from Centrifuge Data. Journal of Petroleum Science and Engineering 135, 577-582 (2015) https://doi.org/10.1016/j.petrol.2015.10.019
19. Wei Xu; Hang Huang; Shi-Zhen Ke; Jin-Peng Li; Hai-Feng Zhang; Yu-Bo Hu. An integral method for calculation of capillary pressure based on centrifuge data of tight sandstone. Petroleum Science 19, 1, 91-99 (2022): https://doi.org/10.1016/j.petsci.2021.10.013
20. McPhee C.; Reed J.; Zubizarreta I. (2015). *Core Analysis - A Best Practice Guide*. Volume 64 Elsevier. Amsterdam, Netherlands.
21. Vuolo J. H. *Fundamentos da Teoria de Erros*. Editora Edgard Blucher Ltda, 2a edição (1996).